Development of a hybrid magnetic resonance/computed tomography-compatible phantom for magnetic resonance guided radiotherapy

Min-Joo Kim[1,2], Seu-Ran Lee[2], Kyu-Ho Song[3], Hyeon-Man Baek[4], Bo-Young Choe[2] and Tae Suk Suh[2],*

[1]Department of Radiation Oncology, Yonsei Cancer Center, Yonsei University College of Medicine, Yonsei University Health System, Seoul, 120-752, Korea
[2]Department of Biomedical Engineering, Research Institute of Biomedical Engineering, The Catholic University of Korea College of Medicine, Seoul, 137-701, Korea
[3]Department of Radiology, Washington University, Saint Louis, Missouri, 63130, United States
[4]Department of Health Sciences and Technology, GAIHST, Gachon University, Incheon, 21999, Korea
*Corresponding author. Department of Biomedical Engineering, Research Institute of Biomedical Engineering, College of Medicine, The Catholic University of Korea, 505 Banpo-dong Seoch-gu Seoul Korea 137-701. Tel: +82-22284361; Fax: +82-2-2258-7506; Email: suhsanta@catholic.ac.kr
(Received 10 January 2019; revised 12 May 2019; editorial decision 24 November 2019)

ABSTRACT

The purpose of the present study was to develop a hybrid magnetic resonance/computed tomography (MR/CT)-compatible phantom and tissue-equivalent materials for each MR and CT image. Therefore, the essential requirements necessary for the development of a hybrid MR/CT-compatible phantom were determined and the development process is described. A total of 12 different tissue-equivalent materials for each MR and CT image were developed from chemical components. The uniformity of each sample was calculated. The developed phantom was designed to use 14 plugs that contained various tissue-equivalent materials. Measurement using the developed phantom was performed using a 3.0-T scanner with 32 channels and a Somatom Sensation 64. The maximum percentage difference of the signal intensity (SI) value on MR images after adding K_2CO_3 was 3.31%. Additionally, the uniformity of each tissue was evaluated by calculating the percent image uniformity (%PIU) of the MR image, which was 82.18 ±1.87% with 83% acceptance, and the average circular-shaped regions of interest (ROIs) on CT images for all samples were within ±5 Hounsfield units (HU). Also, dosimetric evaluation was performed. The percentage differences of each tissue-equivalent sample for average dose ranged from −0.76 to 0.21%. A hybrid MR/CT-compatible phantom for MR and CT was investigated as the first trial in this field of radiation oncology and medical physics.

Keywords: magnetic resonance image; computed tomography; magnetic resonance guided radiotherapy; tissue equivalent; radiation dose calculation

INTRODUCTION

Conventionally, radiation treatment planning uses computed tomography (CT) for standard imaging since CT images offer high geometrical accuracy. The direct connection between the Hounsfield unit (HU) and electron density information for each tissue for dose calculation is the ultimate goal of using CT images in radiation treatment planning [1–3]. However, treatment planning using CT alone is insufficient to accurately delineate the target volumes of some clinical sites.

The use of magnetic resonance (MR)-only based radiotherapy with the application of MR images in the radiation treatment planning process for target delineation has increased because MR images offer superior soft tissue contrast compared to CT images, especially for head and neck tumors, prostate cancer, lung tumors and brain lesions; many studies have been performed with MR-only radiotherapy [4–12]. However, a critical challenge for MR-only radiation treatment is the lack of electron density information for each tissue in the MR

image for dose calculation [13–16]. Additionally, utilization of CT for radiation dose calculation and MR for target delineation are time-consuming processes with extra costs to acquire multiple images. Furthermore, image registration accuracy remains a problem when using MR images for planning radiation treatment [17–19]. With the increasing challenge of MR image-based radiotherapy, several approaches have been proposed to resolve the controversial issues described above, such as the development of multi-modal registration techniques to reduce registration errors and the generation of pseudo-CT images to calculate the radiation dose [3, 5–7, 9, 10, 13–18, 20–27]. However, most related studies, in which image registration between MR and CT images is perfectly performed and conversion of MR images into CT-like images containing electron density information is successfully achieved, both MR and CT images are still required for every patient and demonstrate fractionation during MR-based radiotherapy because of the lack of electron density information from MR images.

Most commercial quality assurance (QA) phantoms used in the radiation oncology field are used for CT calibration and consist of various tissue- or water-equivalent materials. CT of commercialized QA phantoms with various tissue-equivalent materials has been utilized to demonstrate the relationship between HU and electron density to enable the radiation dose to be calculated using a treatment planning system (TPS). Based on the relationship between HU and electron density, the HU value on treatment planning CT, usually kilovoltage fan-beam CT, is converted into electron density and is then applied for dose calculation using a TPS. During the installation process of each CT machine and also the commissioning process of a new TPS in a department of radiation oncology, the relationship between HU to relative electron density (RED) is generated and adopted into the TPS. The relationship between RED and HU is considered to be an important basic parameter for radiation dose calculation even though large differences and uncertainty in converted RED has little impact on dose calculation in most of circumstances [28, 29]. Tissue-equivalent materials for CT images can be easily adopted to develop QA phantoms because the requirements of tissue-equivalent materials on CT images are mainly the physical or electron density of each material. These requirements for CT images can be simply adjusted using materials of various densities. Also, commercialized CT QA phantom has contained various tissue-equivalent materials and. On the other hand, production of tissue-equivalent materials on MR images could be challenging compared to producing tissue-equivalent materials on CT because the principle of MR image acquisition is much more complex than that of CT image acquisition. Only a few studies have reported human, tissue-like imaging using in-house phantoms, including tissue-equivalent materials, and tested the developed phantoms using 1.5 and 3.0 T MR [30–33]. In another study, application of tissue-equivalent materials on MR images for CT image acquisition has been performed only for evaluating multi-modality image registration techniques with the purpose of developing adaptive MR-guided radiation therapy [34]. To the best of our knowledge, other possible applications of those tissue-equivalent materials in the field of radiation oncology have not been reported.

We have hypothesized that a single phantom, a hybrid MR/CT-compatible phantom, used to acquire MR and conventional CT images can be applied for MR-only radiation treatment and used for target delineation and radiation dose calculation. Since various tissue-equivalent samples for each MR and CT image have been developed and inserted in the hybrid MR/CT-compatible phantom, the region of interest (ROI) from a single sample on MR and CT images could represent tissue-equivalent measured data for each signal intensity (SI) on the MR image and HU on the CT image. In addition, the relation between the SI and HU from the same sample image section can be directly applied in a conventional TPS and workflow. Instead of a CT conversion table in the TPS, the relation between the SI and HU can be inserted and converted from the SI on MR to HU on CT or RED. Also, we expect that the developed phantom could be utilized during the commissioning process for an MR-only treatment facility and periodical QA in terms of image values using a density table of CT QA from radiation oncology. Based on the strategy described above, development of a hybrid MR/CT-compatible phantom to fully establish MR-only based radiotherapy was proposed, and its characteristics were determined. Thus, a hybrid MR/CT-compatible phantom for MR-only based radiation treatment has been suggested and the tissue-equivalent materials for an MR/CT-compatible phantom were developed and the results are discussed in this study.

MATERIALS AND METHODS
Requirements of a hybrid MR/CT-compatible phantom

Generally, development of an MR phantom should be given much more consideration compared to development a CT phantom because the procedure for MR image acquisition is much more complex than that for CT image acquisition. In addition, most MR phantoms are usually filled with water or copper sulfate for image quality control or MR spectroscopy [35]. However, a MR phantom that can be used in the radiation oncology field is nonexistent, especially for the purpose of radiation treatment planning and radiation dose calculation. Therefore, we proposed the following essential requirements of a hybrid MR/CT-compatible phantom: (1) tissue-equivalent relaxation times of the MR image and HU of the CT image, (2) dielectric properties of MR, (3) homogeneous relaxation times and HU, (4) sufficient strength to fabricate a torso, (5) ease of handling, (6) chemical and physical stability over an extended time and (7) can be used for a wide variety of tissue-equivalent materials [30–33].

Production of tissue-equivalent materials on MR and CT images

Several studies have developed various types of production techniques for tissue-equivalent materials on MR by utilizing various chemical components for MR-related research. [33] In our study, we followed a reference study and production technique since this reference study determined the complex chemical composition required for tissue-equivalent materials on MR images for various organs in the human body and because the study has been continuously evaluated and updated [32, 33]. The results from the reference study are quantitatively organized, and the chemical components that they used for most human organs have been reported for over 10 years. One of the chemical components used in the reference study was carrageenan,

which was blended from various types of seaweed. Carrageenan was used as a gelling agent to make a rigid gel with sufficient strength to fabricate a torso with good elasticity. Carrageenan is more resistant to cracking than agar gel and can be stored for an extended time. Agaros was used as a T2 modifier, $GdCl_3$ as a T1 modifier, NaN_3 as an antiseptic and 3 g of NaN_3 was added to each sample except the 'Air' sample. NaN_3 is highly soluble in water and very acutely toxic. NaCl and deionized and distilled water were also used. Most organs were mimicked in the study. We selectively chose some organs to be mimicked for MR-only radiation treatment. Table 1, which includes the group 1 samples, lists the selected organs used in our study and the amount of each material. Additionally, to emphasize the advantage of MR-only radiation treatment in terms of soft tissue contrast, we adopted two different chemical compositions for the liver and evaluated the possibility of developing tissue-equivalent materials on each MR and CT image. Based on the group 1 samples, which consisted of 14 different tissue-equivalent materials, we developed group 2 and group 3. Group 2 was designed to evaluate the effectiveness of K_2CO_3 for MR images (14 samples). Group 3 was designed to calculate the change in HU on CT images depending on the amount of K_2CO_3 (8 samples). The specification of groups 2 and 3 are described below.

The chemical component K_2CO_3 was applied to modulate the physical density according to the HU value on CT in each tissue-equivalent material because K_2CO_3 is known to be a component that does not affect MR images [36]. The effectiveness of K_2CO_3 on MR images was tested in our study by calculating the change in SI on MR images between the same tissue-equivalent material with and without K_2CO_3 (group 2). Group 2 consisted of two sets of 7 different tissue-equivalent materials (muscle, white matter, gray matter, spleen, cervix, breast glandular, cartilage), and one of the two sets was developed by adding 15 g of K_2CO_3. The 7 different tissue-equivalent materials in group 2 were determined to be as different as the samples of group 1 among the tissue-equivalent materials in the reference study. To quantitatively evaluate the difference between the group 2 samples with and without K_2CO_3, the percentage change was calculated:

$$Percentage\ change = \left| \frac{SI_{with} - SI_{without}}{SI_{without}} \right| \times 100 \qquad (1)$$

where SI_{with} and $SI_{without}$ are the average SI in circular-shaped ROI of three slices of the MR axial plane from each MR set (7 samples with/without K_2CO_3, respectively).

To determine the amount of K_2CO_3 in each tissue-equivalent material, the change in HU on CT images depending on the amount of K_2CO_3 was calculated using the CT image set of the 8 different samples (group 3). Group 3 consisted of 8 different samples of the same tissue-equivalent material (breast fat, Table 1), and the amount of K_2CO_3 varied from 0 to 100 g (0, 10, 20, 40, 60, 90, 100 and 200 g of K_2CO_3). Additionally, group 3 was utilized to estimate the effect of K_2CO_3 on MR image due to the wide range in the amount of K_2CO_3 used, unlike group 2 that contains 15 g. Each sample set was evenly distributed in the developed phantom to prevent artifacts.

To summarize, each sample group has been developed and specified according to our purposes. Group 1 demonstrates (i) the composition of each organ and (ii) the acceptability of our production process by comparing the T1 and T2 relaxation times with reference data as well as (iii) the background HU value for each organ sample. Measurement of the initial HU value for each tissue-equivalent material of group 1 was performed since the initial HU value required to be modulated using the relation between HU and the amount of K_2CO_3, which would be obtained from the measurement data of group 3. Group 2 was developed to evaluate the effect of K_2CO_3 on MR images. As we described above, the previous group did not utilize K_2CO_3. Thus, evaluation of the effect of K_2CO_3 on MR images was performed using measurement data of group 2. Finally, group 3 was developed to define the amount of K_2CO_3 in each sample required to modulate the HU value on CT, and was also applied to evaluate the effect of a large amount of K_2CO_3 on SI on MR images.

The whole process of developing samples is explained in detail in the reference paper. The mass measurement of each chemical component as well as the mixing and cooling processes are described in the reference paper [37]. The mixing process for each tissue-equivalent material is crucial since carrageenan and agarose, which are gelling agents, are difficult to completely mix before the materials solidify. They can be evenly dissolved at very high temperatures ($>100°C$) [37]. To demonstrate the suitability of our mixing process, the uniformity of each sample was calculated. For each MR image, the percent image uniformity (%PIU) was calculated for all samples using the largest square-shaped ROI on the sagittal plane [35, 38, 39]. This value could be interpreted as uniformity in the vertical direction for each sample and was calculated using equation (2).

$$\%PIU = \left[1 - \left\{ \frac{\overline{S}\max - \overline{S}\min}{\overline{S}\max - \overline{S}\min} \right\} \right] \times 100 \qquad (2)$$

In the selected area, $\overline{S}\min$ was the minimal SI and $\overline{S}\max$ was the maximal SI. The diameter of each ROI was 20 mm and the total number of pixels in the ROI was 448 for one MR image slice. Furthermore, the average HU in circular-shaped ROIs of 7 slices of the CT axial plane image was calculated for each sample as an evaluation of uniformity in the horizontal direction. A difference of ± 5 HU from the average value was defined as an acceptably produced sample in terms of uniformity [40] (Fig. 2).

Design of a hybrid MR/CT-compatible phantom

The developed phantom was designed to hold 14 plugs (diameter: 37 mm; height: 66 mm for the imaging section, airtight container) that contained various tissue-equivalent materials on each MR and CT image. The total height and external diameter were determined according to the internal size of 8 and 32 channels of the MR head-coil, respectively. This phantom was completely watertight, even when it was laid on its side for further utilization (Fig. 1).

MR and CT measurement

Image acquisition using the developed phantom with 14 tissue-equivalent samples of MR images (group 1) and each test sample (groups 2 and 3) mentioned above was performed using a 3.0 T scanner (Achieva Tx 3.0 T, Philips Medical Systems, The Netherlands) with a 32-channel sensitivity encoding (SENSE) head-coil and
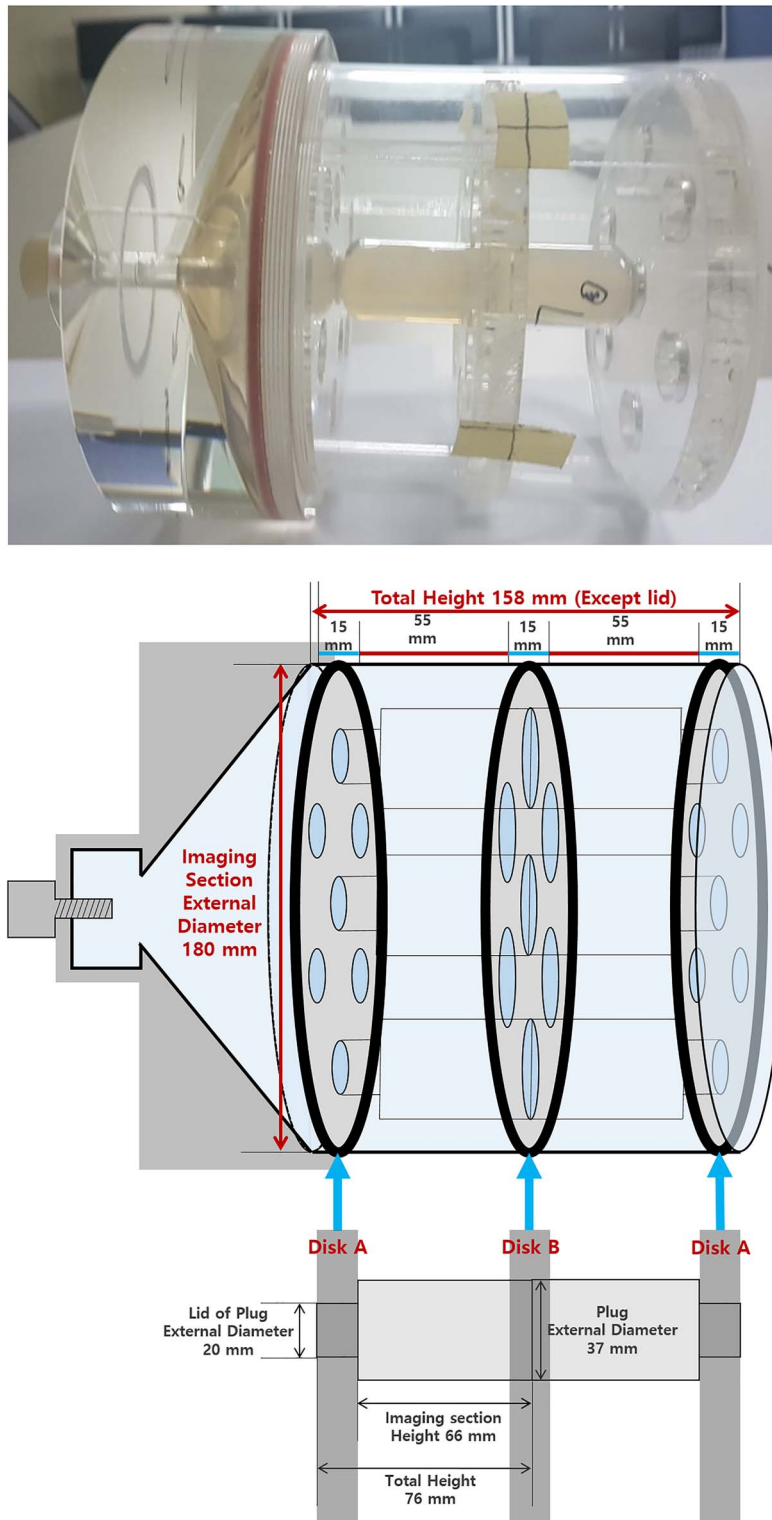
Fig. 1. The developed phantom (top), geometry of the developed phantom (middle) and the location of the plug in the phantom (right). Total height and external diameter were decided by the internal size of the 8-channel MRI head-coil. A disk A at both ends and one disk B in the middle of the phantom can provide two different interspaces. Seven plugs can be located at one of the interspaces between disks A and B. Thus, a total of 14 plugs can be inserted into the phantom. The developed phantom was customized to fix 14 plugs without water leakage.

Table 1. Composition of tissue-equivalent materials for each organ for group 1

Organ	NaCl [w/w%]	Agarose [w/w%]	GdCl3 [μmol/kg]
Muscle	0.291	2.076	29.100
White matter	0.031	0.439	77.600
Gray matter	0.199	0.478	14.700
Liver	0.148	1.315	82.900
Liver	0.148	1.759	84.100
Kidney	0.383	0.981	43.100
Heart	0.323	1.294	27.200
Prostate	0.291	0.714	22.200
Spinal cord	0.039	0.529	59.300
Bone marrow	0.000	0.868	127.700
Breast fat	0.000	0.340	209.400
Pancreas	0.291	1.220	97.600
Air	0.000	0.000	0.000
Water	0.000	0.000	0.000

Table 2. Signal intensity on MR images of various tissue-equivalent materials (group 2)

Organ	Signal intensity		
	With K_2CO_3	Without K_2CO_3	Percentage change
Muscle	1161.45	1130.24	2.8%
White matter	1459.60	1429.54	2.1%
Gray matter	1305.65	1267.97	3.0%
Spleen	1314.30	1285.54	2.2%
Cervix	1244.69	1204.76	3.3%
Breast glandular	1145.79	1139.33	0.6%
Cartilage	1247.81	1213.75	2.8%

CT scanner (Somatom Sensation 64, Siemens Medical Solutions, Forchheim, Germany). The MR image scan parameters for the axial plane were as follows: slice thickness, 10 mm; matrix, 256 × 256; field of view, 220 mm; bandwidth, ±15.63 kHz; and number of acquisitions, 1. The saturation recovery method with a constant TE value of 15 ms was applied for the T1 measurement (TR: 133, 167, 217, 300, 400, 533, 717, 950, 1683, 3000, 5283, 9317 ms). For the T2 measurement, the spin echo method with a constant TR value of 10 000 ms was applied (TE: 15, 22, 29, 39, 52, 69, 93, 125, 167, 224, 300 ms). The sagittal plane of the MR image for the uniformity check of the samples of groups 2 and 3 was acquired using the same scan parameters discussed above with spin echo (fast spin echo, Achieva Tx 3.0 T, Philips Medical Systems, The Netherlands) T2-weighted image TR 15 000 ms and TE 15 ms. The developed phantom was scanned using a CT simulator with a slice thickness of 3 mm and at 120 kVp, 200 mAs, a 50 cm field of view, and a 512 512 image matrix, which resulted in a voxel size of 0.9766 × 0.9766 × 3 mm³ using an axial acquisition.

Dosimetric evaluation

After the development of phantom and tissue-equivalent materials both on CT and MR, T1, T2 measurement of each sample and evaluation of the effect on K_2CO_3 on the MR and CT images, dosimetric

evaluation was conducted using various types of samples on CT and MR images. The CT and MR image from group 1 was applied for dosimetric evaluation. Dose distribution from the CT image of group 1 was utilized as reference data, and dosimetric results from the converted MR image set were imported to a commercialized treatment planning system (RayStation 5 SP3 (5.0.3.17), RaySearch Laboratories, Stockholm, Sweden) and converted to a CT-like image. Dose calculation using the collapsed cone algorithm (Version 3.2) in RayStation was performed by applying 500 cGy on the isocenter of the 6 MV photon for SSD (source to surface distance) 90 cm and 30 x 30 cm² fields with 0° of gantry angle and the isocenter was the center coordinate of the phantom external ROI.

RESULTS
Measurement for MR and CT

Table 1 lists the selected organs and amount of each chemical component required for the production of tissue-equivalent materials. Based on the materials described in Table 1, various tissue-equivalent materials, which were defined in group 1, were produced to evaluate the potential of conversion of the SI on MR into HU on the CT image. A fitted curve using the measured HU values from group 3, which was developed to determine the amount of K_2CO_3 required to modulate
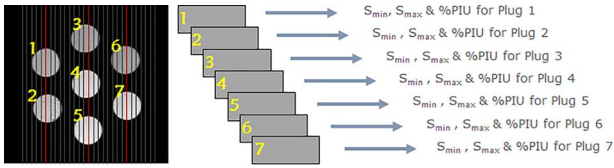
Fig. 2. Schema of the calculation process for percent image uniformity on an MR image. The red line (left) was the selected slices in the MR image to calculate percentage image uniformity (%PIU) and the number (1–7) on each circular shaped region of interest (ROI) indicates each plug with the axial view. The gray rectangle (right, 1–7) indicates the sagittal plane of each plug on the MR image at the selected slice. The selected ROI of the MR image was applied to calculate the signal intensity for minimum and maximum value (S_{min}, S_{max}) and those values were utilized for calculation of %PIU.

HU on CT, is shown in Fig. 3. From the calculated HU shown in Fig. 3, the formula to modulate HU for tissue-equivalent materials on CT images is described below

$$HU = 4.692 \times K_2CO_3(g) + 3.81 \qquad (3)$$

The measured SI from MR for group 2, which was designed to evaluate the effectiveness of K_2CO_3, is shown in Table 2. The maximum percentage difference was 3.31% and the minimum percentage difference was 0.57%. Also, the additional experiment for SI measurement using group 3, which consisted of 8 different samples of the same tissue-equivalent material (breast fat, Table 1) with the amount of K_2CO_3 varying from 0 to 100 g (0, 10, 20, 40, 60, 90, 100 g of K_2CO_3), showed that the maximum percentage difference was 2.75%. The HU, SI and T1 and T2 relaxation times of each tissue-equivalent material listed in Table 1 are shown in Table 3. The differences between the reference data and our measurement data for the T1 and T2 relaxation times were calculated, and the averages of the percentage differences were 0.37 and 5.98% for the T1 and T2 relaxation times, respectively. Also, the initial HU value of each tissue-equivalent material on the MR image was calculated as shown in Table 3. Based on this initial HU value, the appropriate HU of each tissue-equivalent material on the CT image could be produced by considering equation (2).

Production of tissue -equivalent materials

The uniformity of each tissue was evaluated by calculating the %PIU of the MR image and the average and standard deviation of the CT image for all sample images. The %PIU of 83% of the acceptance value for the MR image was 82.18% ± 1.87 [35,38,39]. The average of circular-shaped ROIs on the CT image for all sample was within ±5HU which was the constraint value to evaluate the uniformity of a mixed sample [40]. The durability of the inserted material could be tested since the result was consistent over 4 months. However, each plug that was filled with tissue-equivalent material should be sealed right after the cooling process since the material dries out rapidly. The shape of the solidified material in each plug changes if the caps are not sealed. The end of the cooling process can be seen from the changed color of each material
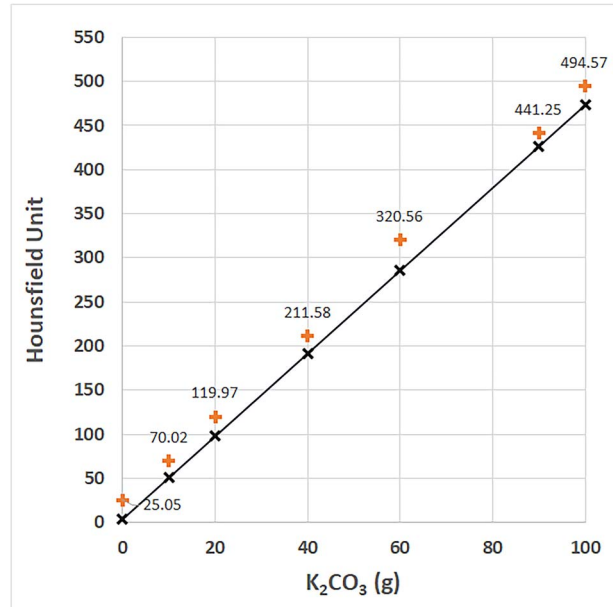

Fig. 3. Relation between the amount of K_2CO_3 and Hounsfield unit.

inside the plugs from the first color of each material to a more yellowish tinge. The time required for the cooling process was about 30 min.

Requirement of a hybrid MR/CT-compatible phantom

The suggested requirements for the hybrid MR/CT-compatible phantom are: (1) tissue-equivalent relaxation times of MR images and HU of CT images, (2) dielectric properties for MR, (3) homogeneous relaxation times and HU, (4) sufficient strength to fabricate a torso, (5) ease of handling, (6) chemical and physical stability over an extended time, and (7) can be used for a wide variety of tissue-equivalent materials. Half of the first requirement was achieved because the tissue-equivalent material for CT images was successfully developed in contrast to the results from MR images. The second requirement could not be investigated in this study. However, the reference research that we followed has demonstrated that the dielectric properties for MR were achieved [32, 33]. The third requirement was also fulfilled for CT images in contrast with the requirement for MR images. The fifth requirement was achieved because of the lightweight feature of the developed phantom due to the weight of the 2D dosimetric measurement equipment for the QA and Catphan phantoms (Phantom Laboratory, Salem, NY, USA), which is the standard phantom for QA for CT images in radiation oncology departments in most hospitals, and ranges from 7 to 33 kg [41, 42]. Next, the stability of the developed phantom was determined as described in 'Production of tissue-equivalent materials' in the Results section since the results were consistent for over 4 months. The last requirement was also accomplished by developing 14 different tissue-equivalent materials. The commercial CT calibration phantom offers 5–7 different tissue-equivalent materials [43,44]. The developed phantom design is illustrated in Fig. 1.

Table 3. Hounsfield unit, signal intensity and T1 and T2 relaxation times of tissue-equivalent material for each organ (group 1). The signal intensity was calculated based on the MR image by applying the scan parameters for the axial plane as follows: slice thickness, 10 mm; matrix, 256 × 256; field of view, 220 mm; bandwidth, ± 15.63 kHz; and number of acquisitions, 1 with TR 10 000 ms, TE 69 ms.

| Organ	Hounsfield unit	Signal intensity	T1			T2		
			Reference (ms)	Measurement (ms)	Percentage Difference	Reference (ms)	Measurement (ms)	Percentage difference
Muscle	5.87	327.81	1420.00	1436.00	−1.11%	32.00	35.41	−9.63%
White matter	0.95	1006.29	832.00	792.70	4.96%	80.00	84.2	−4.99%
Gray matter	2.29	973.98	1820.00	1868.00	−2.57%	99.00	90.5	9.39%
Liver	1.85	549.27	812.00	860.00	−5.58%	42.00	42.39	−0.92%
Liver	1.56	409.71	809.00	841.00	−3.80%	34.00	38.67	−12.08%
Kidney	2.07	655.72	1194.00	1270.30	−6.01%	56.00	64.54	−13.23%
Heart	2.07	643.62	1471.00	1382.00	6.44%	47.00	47.84	−1.76%
Prostate	0.62	922.35	1597.00	1561.00	2.31%	74.00	82.1	−9.87%
Spinal cord	−3.15	953.68	993.00	989.00	0.40%	78.00	86.6	−9.93%
Bone marrow	−1.54	679.68	586.00	595.30	−1.56%	49.00	55.69	−12.01%
Breast fat	−3.46	1013.94	367.00	344.50	6.53%	53.00	56.6	−6.36%
Pancreas	1.51	576.83	725.00	758.40	−4.40%	43.00	43.18	−0.42%
Air	−993.15	1338.00						
Water	3.88	7.00						
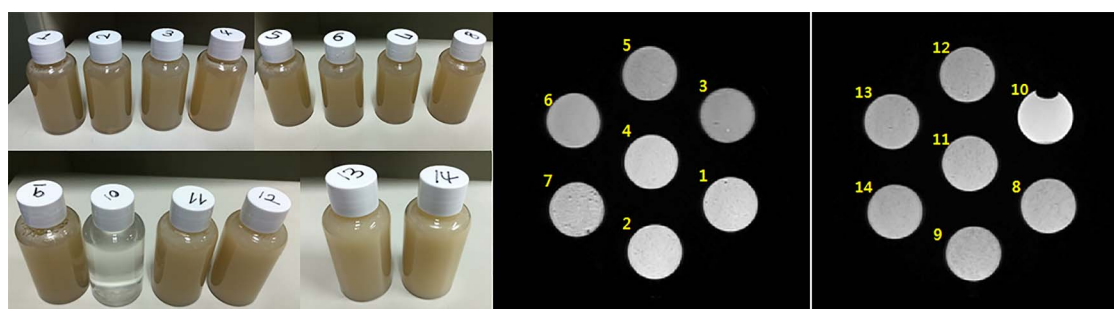
Fig. 4. Fourteen different developed tissue-equivalent materials (left) and its MR image for each plug listed in Table 1 with TR 15 000 ms, TE 15 ms. 1 White matter, 2 gray matter 3 muscle, 4 liver-1, 5 liver-2, 6 kidney, 7 heart, 8 prostate, 9 spinal cord, 10, water 11 bone marrow, 12 pancreas, 13–14 breast fat. The air plug listed in Table 1 is not shown in this figure. Number 14 plug was replaced with an air plug in the final experiment.)

Dosimetric evaluation

Dosimetric results for the converted MR image set was evaluated by comparing dose distribution from the CT image. The percentage difference of each sample for average dose was calculated. The percentage difference ranged from −0.76 to 0.37%. Differences in dose distribution from CT and MR images are illustrated in Fig. 5. The relative dose scale on the figure was selected to be from −5 to 5% for maximum dose.

DISCUSSION

A hybrid MR/CT-compatible phantom for use in the radiation oncology field was designed for MR-only radiotherapy, allowing full application of MR images, including image target delineation and radiation dose calculation without the use of CT. We have aimed to demonstrate that the relation between MR and CT could be directly applied in a conventional TPS because conversion from the SI on MR to HU or RED was possible by using a CT conversion table instead of HU to RED, which can be easily adopted in the clinic. We expect that during operation of an MR-only treatment facility, each clinic would be able to establish a conversion table using MR and CT of the developed phantom and periodically perform QA for the conversion process. To our knowledge, this study was the first trial to design and suggest a method for the development of a hybrid MR/CT-compatible phantom and for use of the phantom image in various applications,
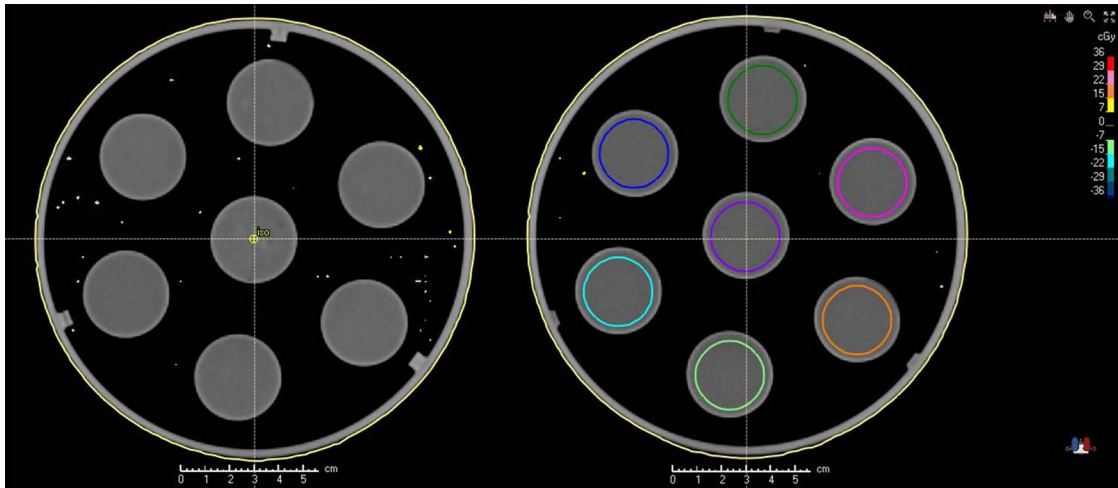
Fig. 5. Dose difference from CT and MR image-based dose distribution. Two slice images were selected and the relative dose scale on the figure was selected from −5, −4, −3, −2, −1, 0, 1, 2, 3, 4, 5% for maximum dose.

Table 4. Dosimetric result for each sample from CT and converted MR image set. Dose–volume histogram of each sample ROI was utilized and $D_{99\%}$ and $D_{1\%}$ were the doses for 99% and 1% of the volume displayed on the cumulative dose volume histogram, which were considered the minimum and maximum doses for each ROI

Organ	With CT image (cGy)			With MR image (cGy)			Percentage difference (%)
	Average	$D_{99\%}$	$D_{1\%}$	Average	$D_{99\%}$	$D_{1\%}$	
Muscle	690	643	717	690	642	717	0.00%
White matter	664	620	693	664	620	693	0.00%
Gray matter	469	407	579	468	406	579	0.21%
Liver	529	484	577	530	485	577	−0.19%
Liver	667	624	697	667	624	697	0.00%
Kidney	598	538	641	598	538	641	0.00%
Heart	652	609	681	652	607	681	0.00%
Prostate	528	479	618	532	476	619	−0.76%
Spinal cord	654	608	686	654	608	686	0.00%
Bone marrow	684	654	709	684	654	708	0.00%
Breast fat	536	483	620	536	482	620	0.00%
Pancreas	528	476	620	528	475	618	0.00%
Air	0	0	0	0	0	0	0.00%
Water	561	485	574	560	483	574	0.18%

such as treatment planning for the contouring process and generating electron density information. The suggested requirements for the hybrid MR/CT-compatible phantom described in the Results section were mostly met in this study, with some exceptions. These aspects will be discussed below. Furthermore, design and production of the whole phantom was successfully conducted in this study.

Modulation of CT images by adding K_2Co_3 was successfully demonstrated in our study. The amount of K_2CO_3 required to produce tissue-equivalent materials for CT images was determined, which was described in equation (3). Additionally, the effect of K_2CO_3 on MR images was investigated, and no considerable effect was found

for MR images since all of the measurement data from group 2 were acceptable for modulation of MR images by adding K_2CO_3, with a 5% percentage difference tolerance (Table 2). However, one of the limitations of this research is that the production technique that used mixed chemical components to make tissue-equivalent materials for MR and CT images has limitations for utilization during MR-only radiation treatment at certain anatomical sites. Since adding chemical components into distilled water could increase the physical density to >1, this increment can directly produce an HU value >0. Certain anatomical sites, especially air regions that have an HU value <0, could not be simulated using this technique. Nonetheless, because

the most important component of MR-guided RT is the superior soft tissue contrast of MR images to clinically verify the tumor region and organs at risk (OARs), the limitation in terms of the air region could be overcome by applying this method to non-air region sites, especially the brain and abdomen. These brain and abdomen sites, except in the upper part of the liver, are filled with soft tissue that mostly lacks air regions due to the introduction of magnetic field distortion at tissue–air interfaces [4, 10, 23]. These clinical sites could maximize the advantage of RT using MR images for the reasons described above. Furthermore, liver cancer is one of the main targeted cancer types that emphasize the major advantage of MR-only radiation treatment. MR images were able to distinguish the specific differences in liver tissue, and our reference data were used to develop and measure two different liver tissues with various chemical compositions. Thus, we used two different compositions of tissue-equivalent materials on MR images (Table 1).

The SI from MR images could not be compared with the HU values from CT images based on the same tissue-equivalent material because of differently measured T1 and T2 data compared with the reference study (Table 3). As described in the Results section, the T1 and T2 measurement data were compared with reference data, and the average percentage differences were 0.37 and 5.98% for the T1 and T2 relaxation times, respectively. The maximum percentage difference was 13.23% of kidney for the T2 relaxation time, and the minimum percentage difference was 0.40% of the spinal cord for the T1 relaxation time. According to the 5% percentage difference tolerance (Table 3), 11 measurement sites among 24 were determined to be acceptable, and the tissue-equivalent materials for the liver were acceptable as tissue-equivalent materials. The tissue-equivalent materials that showed >5% difference also showed a small amount of difference in absolute value. For example, the highest percentage difference was observed from kidney and liver samples for T2 relaxation time and the absolute differences of those sample was 8.54 and 4.67 for T2 relaxation time, whereas the percentage difference of the same samples was 13.23 and 12.08%, respectively. This result could be due to several reasons. First, the geometry of the developed phantom could be the reason for the disagreement between the T1 andT2 measurements and reference data. Each plug in the developed phantom was placed ∼19–22 mm from the next plug with regular spacing to avoid artifacts on CT images, and plugs containing high-density materials were evenly distributed. On the other hand, compared with our study, the plug was much more closely arranged in the reference study, which focused on the development of tissue-equivalent materials only for MR images. Furthermore, the diameter of each plug in the reference study was 40 mm, whereas that in our study was 37 mm. Thus, different geometrical information could affect the disagreement between the reference data and T1 and T2 measurements in our study. However, the space between each plug and the diameters of the phantom and each plug used in our study were inevitable choices since the external diameter of the developed phantom was restricted to ∼180 mm because it was located inside the head-coil for MR image acquisition. In addition, the space between each plug was selected to avoid possible artifacts on CT images, as described above. Therefore, the diameter of the phantom and plug inserted in the phantom and its location inside the phantom were restricted to be equal to those of the reference study, thus leading to the disagreement in the T1 and T2 measurements. Another possible reason for

the disagreement in the T1 and T2 measurement data was the use of different machines for MR image acquisition. Several previous studies have suggested that MR machines have a variety of differences for MR images depending on the manufacturer, although most of the input parameters for acquisition of MR images can be specifically chosen. Although almost all possible input parameters were applied in our MR experiment, the different equipment and manufacturers used for the MR experiment could cause disagreement in the T1 and T2 relaxation times. Thus, the development of tissue-equivalent materials for MR images requires further research, and differences can be minimized by considering the above results.

The scan parameter in our study could be useful to measure the proton density (TE: 15 ms, TR: 15 000 ms, short TE to minimize T2 losses, and a long TR to minimize T1 losses), which could represent the percentage of proton concentration in water and the intensity of the MR image could be proportional to proton density [45]. Thus, the proton density using tissue-equivalent materials was acquired and a standardization process of the developed phantom without sequencing technique was performed unless short TE, long TR does not widely apply in the clinic.

Dosimetric evaluation was performed using CT and MR images with group 1 tissue-equivalent materials (Table 4). The maximum percentage differences of dosimetric results using the CT and converted MR image set of the developed phantom was −0.76%. Since the HU value of CT and the SI value of MR are not in fact in a linear relationship, it is difficult to predict the exact conversion process for overlapping parts. Therefore, in this study, in order to consider the continuity of the SI value of the MR image and to minimize the missing SI value or voxel in the conversion process, the conversion method is designed to convert the SI value of a specific section into a single HU value. In this process, the SI values of 100–380, 380–430, 430–560, 560–670, 670–960, 960–980, 980–1200 and 1200–1400 were converted to the HU values of 30, 15, 60, 0, 30, 60, 35 and 45. A certain range of SI values was determined to reduce the overlapping part as much as possible and one single HU value to SI conversion was determined by reference data [44, 46]. Furthermore, this range could be classified by treatment site. By developing various conversion structures depending on treatment sites, it is expected to minimize the overlapping SI section by distinguishing organs located far apart in the same human body. In summary, dose distribution from CT and MR phantom images could not demonstrate dosimetric effect and inhomogeneous distribution of SI value on MR images. However, this final dosimetric result could represent the application of equation (3) to tissue-equivalent materials to modulate HU value and application of the converted MR image set to a commercialized TPS. From this study, the feasibility of the development of tissue-equivalent materials on both CT and MR images in a hybrid phantom was confirmed. Thus, the inhomogeneity of MR images for the human body and the conversion process from MR to CT image, with consideration of the non-linear relationship between CT and MR, is required as a further study.

CONFLICT OF INTEREST

None declared.

REFERENCES

1. Battista Rider VJ. Computed tomography for radiotheraphy planning. *Int J Radiat Oncol Biol Phys* 1979;6:99–107.

2. Jane Dobbs H, Parker RP, Hodson NJ et al. The use of CT in radiotherapy treatment planning. *Radiother Oncol* 1983;1:133–41.

3. Dowling JA, Lambert J, Parker J et al. An atlas-based electron density mapping method for magnetic resonance imaging (MRI)-alone treatment planning and adaptive MRI-based prostate radiation therapy. *Int J Radiat Oncol Biol Phys* 2012;83:e5–11.

4. Fiorentino a CR, Pedicini P et al. Clinical target volume definition for glioblastoma radiotherapy planning: Magnetic resonance imaging and computed tomography. *Clin Transl Oncol* 2013;15:754–8.

5. Lambert J, Greer PB, Menk F et al. MRI-guided prostate radiation therapy planning: Investigation of dosimetric accuracy of MRI-based dose planning. *Radiother Oncol* 2011;98:330–4.

6. Kapanen M, Tenhunen M. T1/T2∗-weighted MRI provides clinically relevant pseudo-CT density data for the pelvic bones in MRI-only based radiotherapy treatment planning. *Acta Oncol (Madr)* 2013;52:612–8.

7. Jonsson JH, Karlsson MG, Karlsson M et al. Treatment planning using MRI data: An analysis of the dose calculation accuracy for different treatment regions. *Radiat Oncol* 2010;5:62.

8. Karlsson M, Karlsson MG, Nyholm T et al. Dedicated magnetic resonance imaging in the radiotherapy clinic. *Int J Radiat Oncol Biol Phys* 2009;74:644–51.

9. Chen L, Price RA, Wang L et al. MRI-based treatment planning for radiotherapy: Dosimetric verification for prostate IMRT. *Int J Radiat Oncol Biol Phys* 2004;60:636–47.

10. Beavis AW, Gibbs P, Dealey RA et al. Radiotherapy treatment planning of brain tumours using MRI alone. *Br J Radiol* 1998;71:544–8.

11. Rasch C, Steenbakkers R, Van Herk M. Target definition in prostate, head, and neck. *Semin Radiat Oncol* 2005;15:136–45.

12. Prabhakar R, Haresh K, Ganesh T et al. Comparison of computed tomography and magnetic resonance based target volume in brain tumors. *J Cancer Res Ther* 2007;3:121–3.

13. Stanescu T, Jans H-S, Pervez N et al. A study on the magnetic resonance imaging (MRI)-based radiation treatment planning of intracranial lesions. *Phys Med Biol* 2008;53:3579–93.

14. Korhonen J, Kapanen M, Keyriläinen J et al. A dual model HU conversion from MRI intensity values within and outside of bone segment for MRI-based radiotherapy treatment planning of prostate cancer. *Med Phys* 2014;41:011704.

15. Kim S-W, Shin H-J, Lee Y-K et al. The feasibility study of MRI-based radiotherapy treatment planning using look up table. *Prog Med Phys* 2013;24:237.

16. Khoo VS, Dearnaley DP, Finnigan DJ et al. Magnetic resonance imaging (MRI): Considerations and applications in radiotherapy treatment planning. *Radiother Oncol* 1997;42:1–15.

17. Roberson PL, McLaughlin PW, Narayana V et al. Use and uncertainties of mutual information for computed tomography/ magnetic resonance (CT/MR) registration post permanent implant of the prostate. *Med Phys* 2005;32:473–82.

18. Dean CJ, Sykes JR, Cooper RA et al. An evaluation of four CT – MRI co-registration techniques for radiotherapy treatment planning of prone rectal cancer patients. *Br J Radiol* 2012;85:61–8.

19. Li GL, Miller RW. Volumetric image registration of. *Biomed Imaging* 2010;1–27.

20. Smit K, van Asselen B, Kok JGM et al. Towards reference dosimetry for the MR-linac: Magnetic field correction of the ionization chamber reading. *Phys Med Biol* 2013;58:5945–57.

21. Santos DM, St Aubin J, Fallone BG et al. Magnetic shielding investigation for a 6 MV in-line linac within the parallel configuration of a linac-MR system. *Med Phys* 2012;39:788–97.

22. Takao M, Sugano N, Nishii T et al. Application of three-dimensional magnetic resonance image registration for monitoring hip joint diseases. *Magn Reson Imaging* 2005;23:665–70.

23. Chen L, Price R a, Nguyen T-B et al. Dosimetric evaluation of MRI-based treatment planning for prostate cancer∗. *Phys Med Biol* 2004;49:5157–70.

24. Barillot I, Reynaud-Bougnoux A. The use of MRI in planning radiotherapy for gynaecological tumours. *Cancer Imaging* 2006;6:100–6.

25. Park PC, Schreibmann E, Roper J et al. MRI-based computed tomography metal artifact correction method for improving proton range calculation accuracy. *Int J Radiat Oncol Biol Phys* 2015;91:849–56.

26. Heerkens HD, Van Vulpen M, Van Den Berg CAT et al. MRI-based tumor motion characterization and gating schemes for radiation therapy of pancreatic cancer. *Radiother Oncol* 2014;111:252–7.

27. Edmund JM, Nyholm T. A review of substitute CT generation for MRI-only radiation therapy. *Radiat Oncol* 2017;12:28.

28. Thomas SJ. Relative electron density calibration of CT scanners for radiotherapy treatment planning. *Br J Radiol* 1999;72:781–6.

29. Constantinou C, James C, Harrington LAD. An electron density calibration phantom for CT-based treatment planning computers. *Med Phys* 1991;19:325–7.

30. Kato H, Kuroda M, Yoshimura K et al. Composition of MRI phantom equivalent to human tissues. *Med Phys* 2005;32:3199–208.

31. Yoshimura K, Kato H, Kuroda M et al. Development of a tissue-equivalent MRI phantom using carrageenan gel. *Magn Reson Med* 2003;50:1011–7.

32. Ikemoto Y, Takao W, Yoshitomi K et al. Development of a human-tissue-like phantom for 3.0-T MRI. *Med Phys* 2011;38:6336–42.

33. Hattori K, Ikemoto Y, Takao W et al. Development of MRI phantom equivalent to human tissues for 3.0-T MRI. *Med Phys* 2013;40:032303.

34. Niebuhr NI, Johnen W, Güldaglar T et al. Technical note: Radiological properties of tissue surrogates used in a multimodality deformable pelvic phantom for MR-guided radiotherapy. *Med Phys* 2016;43:908–16.

35. Price R, Allison J, Clarke G. Magnetic resonance imaging. *Am Coll Radiol* 2015.

36. Umar MN, Khan K, Anjum MN et al. Synthesis and relaxivity measurement of porphyrin-based magnetic resonance imaging (MRI) contrast agents. *J Struct Chem* 2014;55:910–5.

37. Ohno S, Kato H, Harimoto T et al. Production of a human-tissue-equivalent MRI phantom: Optimization of material heating. *Magn Reson Med Sci* 2008;7:131–40.
38. Song KH, Kim SY, Lee DW et al. Design of a fused phantom for quantitative evaluation of brain metabolites and enhanced quality assurance testing for magnetic resonance imaging and spectroscopy. *J Neurosci Methods* 2015;255:75–84.
39. Goerner FL, Duong T, Stafford RJ et al. A comparison of five standard methods for evaluating image intensity uniformity in partially parallel imaging MRI. *Med Phys* 2013;40:082302.
40. Mutic S, Palta JR, Butker EK et al. Quality assurance for computed-tomography simulators and the computed-tomography-simulation process: Report of the AAPM radiation therapy committee task group no. 66. *Med Phys* 2003;30:2762–92.
41. Algebra TXTC. MapCHECK®2 & 3DVH the gold standard for 2D arrays. *World* 2011;1–4.
42. IBA Dosimetry. MatriXX Evolution System. 2013:12.
43. Bissonnette J-P, Moseley DJ, D a J. A quality assurance program for image quality of cone-beam CT guidance in radiation therapy. *Med Phys* 2008;35:1807–15.
44. Gammex. *Tissue Characterization Phantom Model 467.*, 2004.
45. Tofts P. *Quantitative MRI of the Brain: Measuring Changes Caused by Disease.* John Wiley & Sons, LTd., 2003.
46. Kuntz. Kuntz / Kuntz † · Hepatology, Principles and Practice. 2006:1–902.